

# Flow profiles near receding three-phase contact lines: Influence of surfactants

## Supplemental Material

Benedikt B. Straub,<sup>1</sup> Henrik Schmidt,<sup>1</sup> Peyman Rostami,<sup>1,2</sup>  
Franziska Henrich,<sup>1</sup> Massimiliano Rossi,<sup>3,4</sup> Christian J.  
Kähler,<sup>4</sup> Hans-Jürgen Butt,<sup>1</sup> and Günter K. Auernhammer<sup>1,2</sup>

<sup>1</sup>*Max Planck Institute for Polymer Research,  
Ackermannweg 10, D-55128 Mainz, Germany*

<sup>2</sup>*Leibniz-Institut für Polymerforschung,  
Hohe Straße 6, D-01069 Dresden, Germany*

<sup>3</sup>*Department of Physics, Technical University of Denmark,  
DTU Physics Building 309, DK-2800 Kongens Lyngby, Denmark*

<sup>4</sup>*Institute of Fluid Mechanics and Aerodynamics,  
Bundeswehr University Munich, D-85577 Neubiberg, Germany*

(Dated: May 25, 2021)

## CONTENTS

I. Astigmatism Particle Tracking Velocimetry	ii
II. Velocity and deviation fields	iv
References	v

## I. ASTIGMATISM PARTICLE TRACKING VELOCIMETRY

We performed the experiments in two facilities, setup 1 at the Max Planck Institute for Polymer Research in Mainz, and setup 2 at the Institute of Fluid Mechanics and Aerodynamics at the Bundeswehr University Munich. We obtained similar results in both experiments. The final plots for pure water,  $C_{12}E_5$  and 5%CMC  $C_8E_3$  were obtained from setup 1 and the remaining  $C_8E_3$  plots from setup 2.

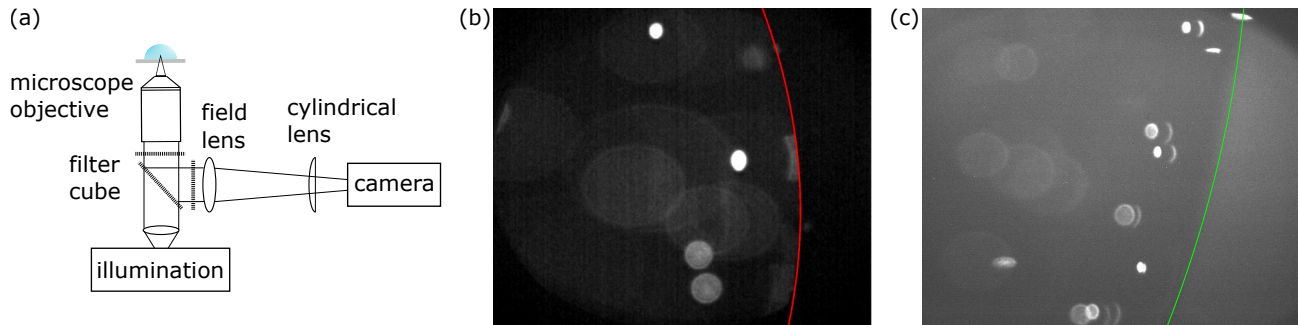


FIG. S1. (a) Sketch of the experimental setups. (b, c) Examples of astigmatic particle images obtained with setup 1 and 2, respectively. The contact line of the drop is highlighted in red or green.

The setup 1 consisted of a Leica DMI 6000B inverted microscope in combination with a Photron Fastcam 1.1. Images were recorded with a recording speed of 50 Hz which provided good spatial and temporal resolution. The optical elements were a  $150\ \mu\text{m}$  achromatic cylindrical lens (Thorlabs) directly in front of the camera sensor and a 40X microscope objective (LUCPLFLN, Olympus, Japan). Illumination was provided by a mercury lamp in combination with an appropriate filter cube to adjust the used wavelength. As tracer particles, red-fluorescent polystyrene spheres with a diameter of  $2\ \mu\text{m}$  were used (microParticles GmbH, PS-FluoRed). Small polystyrene beads are slightly denser than water ( $\rho_{\text{PS}} = 1050\ \text{kg/m}^3$ ). Therefore, to avoid sedimentation of the particles a 1:1 mixture of water and deuterated water was used. Furthermore, the sedimentation time of the particles (even in pure water) is much larger than the time scales of the phenomena investigated, therefore it can safely be assumed that they follow faithfully the fluid flow [S1]. Figure S1 (a) shows a schematic sketch of the setup. The maximum measurement volume of this setup configuration is around  $400 \times 450 \times 60\ \mu\text{m}^3$ .

The detection of the particle position and shape is made in two steps. The first step is a

pre-detection of the particles using a binarized image. In the second step the pre-detection information is used as the start parameter for an iterative two-dimensional Gaussian fitting procedure to the full intensity profile of the particle image. See [S2] for the used Gaussian fit function. The fit parameters of the Gaussian function are the extensions in both direction and middle point of the tracer particles. To minimize errors the fitting is done iteratively with varying segmentation sizes.

To calibrate the system several particles are placed on top of a glass cover slip. A drop of the measurement fluid is placed above the particles without disturbing them. The focus of the microscope objective is moved through the probe with known step sizes. The result is a calibration curve like shown in FIG. 3 (c) of the main article. The fit function for the principal axes with the dependent axial variable  $z$  can be found in [S2].

The particle coordinates are combined to particle trajectories by using the “track” algorithm of Crocker and Grier [S3]. Due to the cylindrical lens the image is also globally deformed. Therefore, the lateral particle coordinates have to be transformed back to an undeformed image. We took pictures of a standard calibration grid (PS20, Pyser Optics, Kent, UK) before and after the introduction of the cylindrical lens into the beam path. We used the “bUnwarpJ” [S4, S5] Plugin of ImageJ [S6–S8] to generate a transformation matrix. We used this matrix to transform the lateral coordinates of the particles back into the undeformed system.

The error estimation was carried out using test data. These test data were measured the same way as the calibration curves. The axial position of the particles is therefore known. The calibration is used on this data and the deviation between the known axial position and the calculated axial position with the calibration is used as the axial error. The axial standard deviation is  $\pm 0.98 \mu\text{m}$  and the estimated lateral uncertainty is  $\pm 0.25 \mu\text{m}$ .

The setup 2 was similar to setup 1 but used different components. Specifically, it consisted of an inverted microscope Axio Observer Z1 (Carl Zeiss AG) in combination with an Imager sCMOS camera (LaVision GmbH), with images also recorded at 50 Hz. The optical elements were a  $150 \mu\text{m}$  cylindrical lens placed also in front of the camera sensor and a 40 X microscope objective (LD Plan-Neofluar, Carl Zeiss AG). The illumination was provided by a high-power green light-emitting diode (LED). As tracer particles, red-fluorescent (Rhodamine B) polystyrene spheres with a diameter of  $4 \mu\text{m}$  were used (synthesized at the Max Planck

Institute for Polymer Research).

To obtain the calibration images for setup 2, a similar procedure as the one described for setup 1 was used. Instead, a different approach was used to obtain the axial coordinate. Rather than comparing the  $x$  and  $y$  extensions, the shape of the measured particle images was directly compared with the shape of the reference particle images by means of the normalized cross-correlation function. More details on this calibration approach are given in [S9]. Also in this case, a standard calibration grid (Thorlabs) was used to map the image distortion and get the coordinates in real units.

The measurement volume obtained with this configuration was about  $380 \times 430 \times 70 \mu\text{m}^3$ , with an estimated uncertainty of  $\pm 0.7 \mu\text{m}$  in the axial direction, and  $\pm 0.1 \mu\text{m}$  in the lateral direction.

## II. VELOCITY AND DEVIATION FIELDS

The deviation field of a 5%CMC  $\text{C}_{12}\text{E}_5$  also shows the discussed deviation close the the free surface and in the bulk flow (Fig. S2 (a)). Although the change in surface tension is very small, it is still a factor 3 higher than the noise level we measured for pure water. We attribute the small systematic variation of the calculated surface tension difference for water to effect of the finite size of our tracer particles. Note that this systematic error has a different dependence on the distance from the contact line and falls off faster.

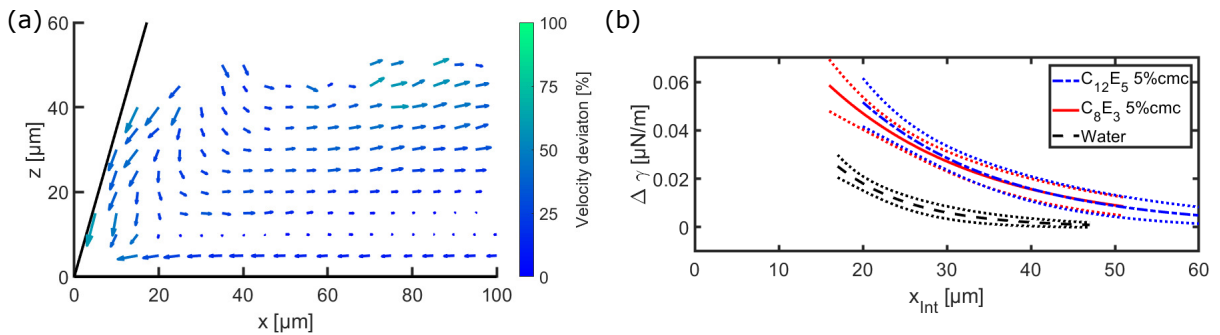


FIG. S2. (a) Deviation field of 5%CMC  $\text{C}_{12}\text{E}_5$  solution. (b) Change in surface tension of water, 5%CMC  $\text{C}_{12}\text{E}_5$  and 5%CMC  $\text{C}_8\text{E}_3$ .

- 
- [S1] M. Rossi, A. Marin, and C. J. Kähler, Interfacial flows in sessile evaporating droplets of mineral water, *Physical Review E* **100**, 033103 (2019).
- [S2] C. Cierpka, M. Rossi, R. Segura, and C. J. Kähler, On the calibration of astigmatism particle tracking velocimetry for microflows, *Measurement Science and Technology* **22**, 015401 (2011).
- [S3] J. C. Crocker and D. G. Grier, Methods of digital video microscopy for colloidal studies, *Journal of Colloid and Interface Science* **179**, 298 (1996).
- [S4] C. O. S. Sorzano, P. Thevenaz, and M. Unser, Elastic registration of biological images using vector-spline regularization, *IEEE Transactions on Biomedical Engineering* **52**, 652 (2005).
- [S5] I. Arganda-Carreras, C. O. S. Sorzano, R. Marabini, J. M. Carazo, C. Ortiz-de Solorzano, and J. Kybic, Consistent and elastic registration of histological sections using vector-spline regularization, in *Computer Vision Approaches to Medical Image Analysis*, Vol. 4241, edited by R. R. Beichel and M. Sonka (Springer Berlin Heidelberg, 2006) pp. 85–95.
- [S6] J. Schindelin, I. Arganda-Carreras, E. Frise, V. Kaynig, M. Longair, T. Pietzsch, S. Preibisch, C. Rueden, S. Saalfeld, B. Schmid, J. Y. Tinevez, D. J. White, V. Hartenstein, K. Eliceiri, P. Tomancak, and A. Cardona, Fiji: an open-source platform for biological-image analysis, *Nature Methods* **9**, 676 (2012).
- [S7] C. A. Schneider, W. S. Rasband, and K. W. Eliceiri, Nih image to imagej: 25 years of image analysis, *Nature Methods* **9**, 671 (2012).
- [S8] C. T. Rueden, J. Schindelin, M. C. Hiner, B. E. DeZonia, A. E. Walter, E. T. Arena, and K. W. Eliceiri, Imagej2: Imagej for the next generation of scientific image data, *BMC Bioinformatics* **18**, 529 (2017).
- [S9] R. Barnkob, C. J. Kähler, and M. Rossi, General defocusing particle tracking, *Lab on a Chip* **15**, 3556 (2015).